Materiales de Construcción (74) 355
July-September 2024, e349
ISSN-L: 0465-2746, eISSN: 1988-3226
https://doi.org/10.3989/mc.2024.368923

Experimental study on mechanical and durability properties of concrete incorporating various polyvinyl alcohol iber lengths and dosages

W. Chen[a,b], Y. Wen[b]✉

a. College of Harbour, Coastal and Offshore Engineering, Hohai University, (Nanjing, China)
b. School of Civil Engineering, Inner Mongolia University of Science and Technology, (Baotou, China)

✉: 200203020011@hhu.edu.cn

Received 30 November 2023
Accepted 13 May 2024
Available on line 31 October 2024

ABSTRACT: To inquire about the properties of concrete reinforced with polyvinyl alcohol (PVA) fiber (various fiber lengths and dosages), different experimental tests including mechanical property, cracking resistance, and chloride resistance were investigated. The overall performance of PVA fiber-reinforced concrete (FRC) was innovatively analyzed integrating mechanical indicators and crack resistance parameters. Furthermore, nuclear magnetic resonance (NMR) and scanning electron microscope (SEM) were selected to analyze the causes and mechanisms underlying the alterations in the performance of PVA-FRC. The experimental results demonstrate that the flexural strength, the crack resistance characteristic and chloride ion penetration resistance of PVA-FRC are significantly improved compared to ordinary concrete. Increasing fiber length plays a key role in flexural strength, compared with fiber dosage. Considering both mechanical properties and durability, PVA-FRC containing 0.25% volume fraction of 12 mm PVA fibers (F12-0.25) demonstrated optimal performance.

KEY WORDS: PVA-FRC; Mechanical properties; Cracking resistance; Chloride penetration; Drying-wetting cycle; NMR; SEM.

Citation/Citar como: Chen W, Wen Y. 2024. Experimental study on mechanical and durability properties of concrete incorporating various polyvinyl alcohol fiber lengths and dosages. Mater. Construcc. 74(355):e349. https://doi.org/10.3989/mc.2024.368923

RESUMEN: *Efecto de la longitud y la dosificación de las fibras de polivinilo alcohol (PVA) sobre las propiedades mecánicas y la permeabilidad a iones cloruro del hormigón.* Para investigar las propiedades del concreto reforzado con fibra de alcohol polivinílico (PVA) (distintas longitudes y dosis de fibra), se realizaron diferentes pruebas experimentales incluyendo propiedad mecánica, resistencia a la fisuración y resistencia al cloruro. El rendimiento general del concreto reforzado con fibra de PVA (FRC) fue analizado de manera innovadora integrando indicadores mecánicos y parámetros de resistencia a la fisuración. Además, se seleccionaron la resonancia magnética nuclear (NMR) y el microscopio electrónico de barrido (SEM) para analizar las causas y mecanismos detrás de las alteraciones en el rendimiento del PVA-FRC. Los resultados experimentales demuestran que la resistencia a la flexión, la característica de resistencia a la fisuración y la resistencia a la penetración de iones de cloruro del PVA-FRC mejoran significativamente en comparación con el concreto ordinario. El aumento de la longitud de la fibra juega un papel clave en la resistencia a la flexión, en comparación con la dosis de fibra. Considerando tanto las propiedades mecánicas como la durabilidad, el PVA-FRC que contiene una fracción de volumen del 0.25% de fibras de PVA de 12 mm (F12-0.25) demostró un rendimiento óptimo.

PALABRAS CLAVE: PVA-FRC; Propiedades mecánicas; Resistencia a la fisuración; Penetración de cloruros; Ciclo de secado-humedad; NMR; SEM.

Copyright: ©2024 CSIC. This is an open-access article distributed under the terms of the Creative Commons Attribution 4.0 International (CC BY 4.0) License.

1. INTRODUCTION

Due to its durability, reliability and affordability (1) , concrete is used in a variety of buildings and structures. However, it is prone to cracking under tensile strain (2, 3). These cracks allow water and chloride ions to penetrate the concrete matrix, accumulating continuously during service. When chloride ion concentration at the rebar-concrete interface reaches the threshold, the passive film on the surface of steel will be broken, simultaneously. This corrosion process gradually weakens the steel, significantly reducing the structure's load-bearing capacity and service life (4, 5). To mitigate crack extension and increase matrix toughness, the chopped fibers are added into matrix performing deflection and bridging roles (6). This type of concrete is classified as fiber-reinforced concrete (FRC).

Steel fiber is commonly used to enhance the tensile properties of concrete. However, it adversely affects the structural quality. Consequently, research has shifted toward synthetic fibers, including glass, polyethylene (PP), and polyvinyl alcohol (PVA) fibers. Glass fiber, however, exhibits poor alkali resistance, while PP fiber suffers from poor dispersion and higher costs. In contrast, PVA fiber offers significant benefits, including being lightweight, alkali-resistant, and possessing high tensile strength, aspect ratio, and modulus of elasticity (7, 8). Notably, PVA fiber contains hydroxyl groups (OH), as showed in Figure 1, providing a nucleation point for strong chemical bonding and the formation of hydration products (9, 10). PVA fiber's high tensile strength significantly aids the matrix in dissipating external loads. Furthermore, PVA fiber transfers energy during crack propagation, thus reducing stress concentration and inhibiting crack growth (10, 11). These advantages underscore PVA fiber's promising potential in infrastructure construction (12).

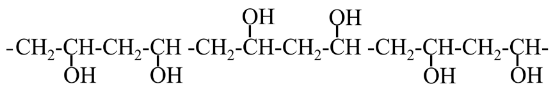

Figure 1. PVA fiber structure

The addition of PVA fiber has been advocated in concrete or cementitious materials to ameliorate deformation and load-bearing performances. For instance, PVA fiber was utilized as an appropriate additive in concrete mixture. Hu (13) analyzed the mechanical properties of plain concrete with varying PVA fiber contents (0-0.116%) and a consistent fiber length of 12.3 mm. They concluded that compressive strength and elastic modulus are positively correlated with the fiber content. Jang (14) investigated the flexural fatigue performance of concrete combining 6 mm PVA fiber with an admixture rate of 0-1.2 kg/m^3, after freeze-thaw damage. They discovered a positive correlation between PVA fiber content and improvements in fatigue bending load and deformation. Wang (15) mixed silica fume and PVA fiber (12 mm and 1.2 kg/m^3) into concrete and investigated the effect of single or mixed additive on performance. Results indicated that the fibers effectively inhibit drying shrinkage and crack development in both concrete and mortar. Additionally, Wu (16) performed dynamic uniaxial compression and split tensile tests on concrete mixed with 12 mm fibers at different volume fractions (0, 0.2, 0.4, and 0.6%). The results shown that brittle properties and residual strength of concrete are improved, which can be attributed to the toughening effect of the PVA fiber. PVA fiber concrete has garnered attention from a multitude of researchers, and it has also been utilized in practical repair projects. For example, PVA fiber concrete has been implied in the 2# trial part of third line ship lock at Zaohe Ship Lock in Jiangsu, China (17). While many studies have been conducted, there is still a gap regarding the consistency of mix proportions combining varying fiber length and dosage.

The primary objective of this study is to elucidate the impact of PVA fibers on the mechanical behavior and durability of concrete. To achieve this, several key properties of concrete, such as workability, flexural strength, cracking resistance, and susceptibility to chloride ion penetration, were investigated. This study innovatively clarified the comprehensive performance of PVA fiber-reinforced concrete (PVA-FRC) by integrating mechanical indicators with crack resistance parameters. Subsequently, samples that exhibited superior comprehensive performance were further analyzed through chloride ion penetration tests to validate their enhanced durability. Additionally, to delve deeper into the microstructural effects, nuclear magnetic resonance (NMR) and scanning electron microscopy (SEM) techniques were employed. These methods provided a visual examination of the density and microstructure of the specimens, aiming to uncover the underlying mechanisms through which PVA fiber enhances concrete performance.

2. EXPERIMENTAL PROGRAM

This section outlines the experimental framework, detailing the selection of raw materials, specimen preparation protocols, exposure scenarios, and testing methodologies. Given the significant variations in fiber dosages reported in the literature, which complicates their selection for practical applications (13, 16, 18). To overcome these challenges, this study adheres to the dosage recommendations specified in the PVA fiber Manufacturers' Instructions. Consequently, the PVA volume fractions were set at 0.05%, 0.15%, and 0.25%. In this study, the water-binder ratio was fixed at 0.43. Detailed descriptions of the investigations follow.

2.1. Raw materials

Cement (1. P.O 42.5) and Class I fly ash, substituting 10% of the cement's mass, served as the binder materials. Tables 1 and 2 detail the physical and chemical properties of these binders, respectively. The gravel, featuring a maximum particle size of 12 mm, was chosen as the coarse aggregate to optimize fiber dispersion and the requirement of slab test (15, 19). Additionally, the river sand with a fineness modulus of 2.4 was used in PVA-FRC as fine aggregates. The remaining physical properties of coarse aggregate included a moisture content of 0.17% and a crushing index of 8.2%. In addition, the coarse and fine aggregates were sourced from Inner Mongolia Huameng Aggregate Co., Ltd. (Inner Mongolia, China), with bulk densities of 2750 $kg \cdot m^{-3}$ and 2510 $kg \cdot m^{-3}$, respectively. Tap water was used for casting and curing all concrete mixtures, ensuring that the maximum chloride content did not exceed 500 ppm. To adjust fluidity performance, the dosage of naphthalene sulfonate superplasticizer (NSS) was 1.4% of the binder material mass, which is supplied by Baotou Anshun New Building Materials Co., Ltd (Inner Mongolia, China) (20). The NSS dosage remained consistent to explore the impact of PVA fiber length and dosage on concrete workability. The microscopic morphology and mechanical parameters of the PVA fiber are illustrated in Figure 2 and Table 3, respectively.

Table 1. Properties of binders.

Composition		Cement	Fly ash
Specific surface ($m^2 \cdot g^{-1}$)	-	360	475
Loss of ignition	-	0.88	3.17
0.045 mm sieve residue	-	-	0.11
Specific gravity ($g \cdot cm^{-3}$)	-	3.23	2.69
Setting time (min)	initial	95	-
	final	216	-
Compressive strength (MPa)	3 days	24.80	-
	28 days	48.50	-

-indicate that the data mentioned above was not tested in this article.

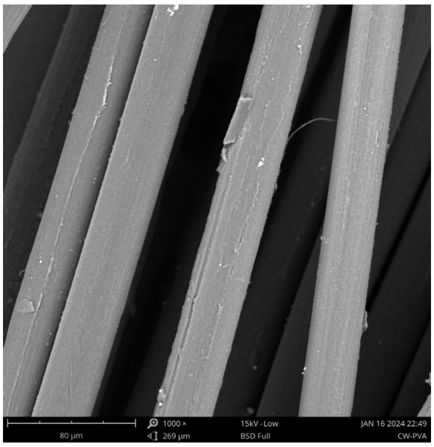

Figure 2. Microscopic morphology of PVA fiber.

Table 2. Chemical compositions of the binders.

Composition (%)	Cement	Fly ash
SiO_2	22.39	48.83
Al_2O_3	7.16	17.18
Fe_2O_3	2.49	8.07
CaO	53.26	4.23
MgO	4.32	6.76
SO_3	1.30	2.16

Table 3. Properties of PVA fiber.

Diameter (mm)	0.035
Length (mm)	8, 12, 18
Aspect ratio	229, 343, 514
Elastic modulus (GPa)	42
Tensile strength (MPa)	1600
Density ($g \cdot cm^{-3}$)	1.2
Elongation (%)	8
Color	white
Fiber surface	smooth

2.2. Mixture proportions

Nine PVA-FRC mixtures incorporating lengths of 8 mm, 12 mm and 18 mm at volume fractions of 0.05%, 0.15% and 0.25% were prepared. An ordinary concrete mix, referred to as NC, was utilized for comparison purposes. The proportions of a typical PVA-FRC and NC, as shown in Table 4, were determined and compared.

2.3. Specimen preparation and testing

To enhance dispersibility, PVA fiber was premixed in water as part of the pretreatment process. Binders and aggregates were dry-mixed for three minutes. Then, water containing dispersed PVA fiber and NSS was added and mixed for an additional three minutes. Finally, the mixture was vigorously stirred for an additional five minutes to ensure optimal fiber dispersibility. Upon completion of the mixing process, the fresh mixtures of each type were cast into prismatic, cubic and steel plate molds. Only one specimen was cast in the steel plate mold, while the others were poured into three parallel specimens. The type and dimensions of the cast specimens are listed in Table 5. Concurrently, the specimens were covered with plastic wrap to minimize water evaporation. After being left outside for one day, the samples were demolded. All specimens were placed in a standard curing chamber at 20±2 °C with a relative humidity of 95% and continued to cure for 27 days.

2.3.1. Workability

Following the Chinese standard GB/T 50080-2016 (21), the slump test for each type of proportion was carried out using a truncated conical slump cone after concrete mixing. This slump cone has an upper diameter of 100 mm, a lower diameter of 200 mm, and a height of 300 mm. Additionally, the initial uniform dispersion of fibers was assessed solely through visual inspection, as this method is considered reasonable and used only for preliminary assessments (22, 23).

2.3.2. Flexural strength

According to the CECS 13-2009 (24), a three-point bending test was performed on prismatic samples of each mixture measuring 100×100×400 mm^3 after standard curing to assess the impact of PVA fiber on the flexural strength (Fs). The schematic diagram of the test piece and loading mode is depicted in Figure 3. The average of three experimental results was utilized as the representative value for Fs.

Table 4. PVA-FRC mixture proportions.

Mixture	PVA fiber		Cement (kg/m^3)	Fine aggregate (kg/m^3)	Coarse aggregate [b] (kg/m^3)	Fly ash (kg/m^3)	Water (kg/m^3)	NSS (kg/m^3)
	Length (X)(mm)	Volume fraction (Y)(%)						
NC	-	0	330	837	1061	61	170	5.449
FX-Y [a]	8 mm 12 mm 18 mm	0.05 0.15 0.25						

[a] X and Y indicate fiber length and fiber dosage, respectively.
e.g. F8-0.05 indicates mixture with 8 mm and 0.05% PVA fiber and NC indicates normal concrete.
[b] maximum particle size is 12 mm.

Table 5. The type and dimensions of specimens.

Type	Nominal size	Function	Numbers[a]
Prismatic	100×100×400 mm^3	Flexural strength	3
Steel plate mold	600×600×63 mm^3	Cracking resistance	1
Cubic	100×100×100 mm^3	Chloride penetration depth	3
		Chloride content	3

[a] indicate the number for each type mixture.

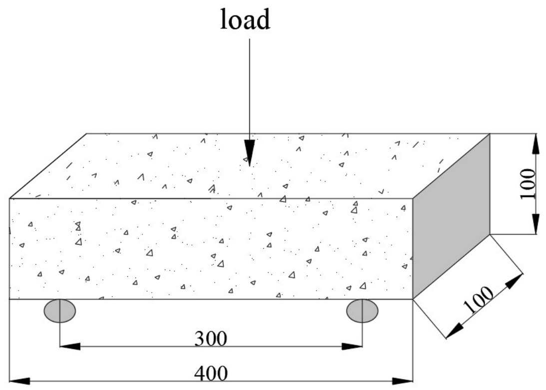

Figure 3. Geometry of three-point bending.

2.3.3. Cracking resistance

To estimate the crack resistance potential, the mixture of each type was molded into a steel plate mold measuring 600×600×63 mm^3, as shown in Figure 4(a). According to the Chinese standard CECS 38-2004 (20), a fan was positioned horizontally in the middle of the mold to maintain the desired ambient evaporation rate. During the whole test, a constant wind speed of 5-7 m·s^{-1} was maintained, as illustrated in Figure 4(b). After 24 h exposure test, the crack area is calculated by Equation [1] and the index indicating of anti-crack property is calculate by Equation [2]. For each specimen, the crack length and width were recorded, detected using a width measuring instrument (JW-CK102), and analyzed with Image J software.

$$A = \sum_{i=1}^{n} w_{i,\max} l_i \qquad [1]$$

$$\eta = \frac{A_m - A}{A_m} \qquad [2]$$

where, A is the crack area of PVA-FRC, mm^2; A_m is crack area of the normal concrete, mm^2; $w_{i.\max}$ is the maxim width of the number i crack, mm; l_i, is the length of the number i crack, mm; η is the index of anti-cracking property.

2.3.4. Drying-wetting cycles

An accelerated cycle mechanism was designed to simulate the service conditions of concrete in a hot-wet climate. Three cubic specimens of each type mixture were selected to undergo dry-wet cycles test. The cube specimen measuring 100×100×100 mm^3, had only one surface exposed during the chloride ion dry-wet cycle test, while the other surfaces were coated with epoxy resin. A dry-wet cycle was described as below: initially, the concrete specimen was immersed in sodium chloride solution with mass fraction 3.5% for 7 days. Subsequently, the specimen was allowed to dry in the natural environment for 7 days. After the corresponding period, 2 cycles (28 days), 4 cycles (56 days), 6 cycles (84 days) and 8 cycles (112 days), the penetration depth of chloride ion and free chloride ion content in the sample were measured and calculated. The pH of the solution was regularly checked, a critical step in ensuring a constant concentration.

2.3.5. Chloride penetration depth testing

The depth of chloride penetration in the cubic specimen was measured after the cycles. A wet stone

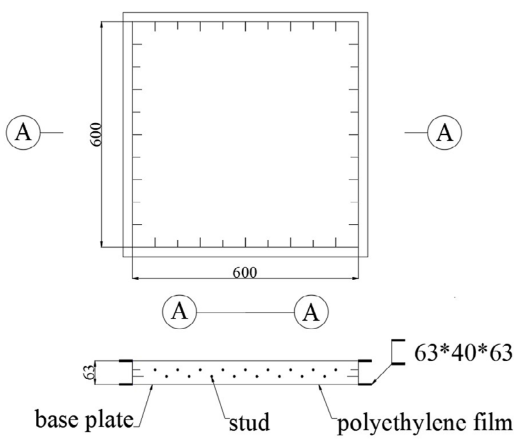

(a) The diagrammatic drawing of slab.

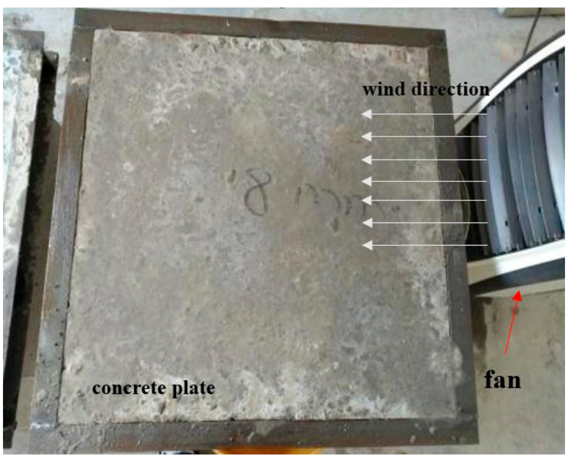

(b) The modelling concrete of slab.

Figure 4. Geometry of cracking resistance test.

cutter was used to cut 5 mm thick slices from the exposed surface of the cubic sample under test, to ensure the accuracy of measurements. The surface of each slice was sprayed with a 0.05 mol/L potassium chromate indicator solution and then dried at 105 °C for 2 hours. This spraying and drying process was repeated once. Finally, the dried sample slice was sprayed with a 0.1 mol/L solution of silver nitrate. The area of color development was divided into 10 equal sections across the width (100 mm), and the depth from the surface to each division was measured with calipers. The average of these measurements was defined as the chloride corrosion depth (25).

2.3.6. Chloride content testing

Powder samples were collected from four different positions at the same depth in the cubic specimen after the drying-wetting cycles. The depth intervals for collecting powder were set as follows: 1) every 1 mm up to a depth of 10 mm; 2) every 2 mm beyond 10 mm depth. A sieve with a mesh diameter of 0.15 mm was used to screen the powder samples. The test procedure depicted in Figure 5 adheres to the Chinese standard JTS/T 236-2019 (26). Subsequently, the apparent chloride diffusion coefficient was calculated using Fick's second law.

2.3.7. NMR test

The NC, F12-X, and F18-X series samples, each with a diameter and height of 50 mm, were subjected to a vacuum water retention pressure of 0.1 MPa for 16 hours using the NMR instrument (MesoMR23-060V-I). The experiment was conducted in a laboratory maintained at 25±0.2 °C to control temperature effects on the test results. Mathematical models relating relaxation time to pore-specific surface area and volume can be developed based on the rapid exchange theory. According to this theory, there is a linear relationship between the transverse relaxation time (T_2) and pore size (27, 28). The value of T_2 can be approximately calculated as expressed in Equation [3].

$$\frac{1}{T_2} = \rho_{2,sur} \times \frac{S}{V} = \rho_{2,sur} \times \frac{2}{r} \quad [3]$$

where, T_2 is the relaxation time of water in the pore; $r_{2,sur}$ is the T_2 surface relaxivity; r is the radius of the pore; S/V is the pore surface area-volume ratio, which can be equal to $2 \cdot r^{-1}$ in this research.

2.3.8. SEM test

The SEM instrument (FEI Quanta 650FEG) was used and testing sample measuring 5×5 mm^2 was treated by epoxy resins to close the internal pores of the material (29). Then, sample was cut and polished to examine the microstructure.

3. RESULTS AND ANALYSIS

3.1. Workability

The significantly different slump of each mixture is shown in Figure 6. It is apparent that workability inversely correlates with the incorporation of fibers. Specifically, maintaining constant fiber length, an increase in fiber dosage invariably leads to a reduction in slump. Practically speaking, greater fiber content correlates with a decreased slump, although employing an appropriate vibration technique can enhance the placement and uniformity of fiber-reinforced concrete, as referenced in (30). In this study, with a fiber content of 0.25%, the slump value does not exceed 10 mm. Comparisons of this series of mixture proportions with others have not been conducted. The relationship between the slump and the addition of two

Figure 5. The flowchart of chloride ion determination.

other fiber dosages is elucidated and depicted through a normalized folding line. Notably, the slump reduction is significant in the concrete series with 0.15% fiber content compared to others. Such as, comparing FX-0.05 with FX-0.15, the fiber dosage varying from 8 mm to 18 mm, the slump decreased by Such as, comparing FX-0.05 with FX-0.15, the fiber dosage varying from 8 mm to 18 mm, the slump decreased by 10.6%, 25.5%, and 47.8% respectively, all demonstrating poorer flowability compared to NC., 25.5%, and 47.8% respectively, all demonstrating poorer flowability compared to NC. Evidently, PVA fiber detrimentally affects workability. This decrease in slump can be attributed to the reduced efficacy of cement in binding coarse aggregates and the obstruction caused by the three-directionally randomly distributed fiber grid, which impedes fluidity (31). In addition, the hydroxyl groups on PVA fiber surface tend to absorb water, thereby reducing the free flow of water between particles (32, 33).

3.2. Flexural strength

The test results for flexural strength (Fs) are comprehensively detailed in Figure 7. To facilitate comparison, the Fs of each specimen has been normalized to that of normal concrete (NC), denoted as normalized f_f=1. All specimens exhibit a consistent increase in Fs across various fiber lengths and dosages. Nevertheless, the impact of 8 mm fibers on Fs is notably minor compared to fibers of 12 mm and 18 mm lengths, particularly at lower volumetric dosages. Specifically, the specimens designated F8-0.05 and F8-0.15 demonstrate equivalent flexural strength values. When the volume fraction is minimal, variations in parameters appear to exert a negligible influence

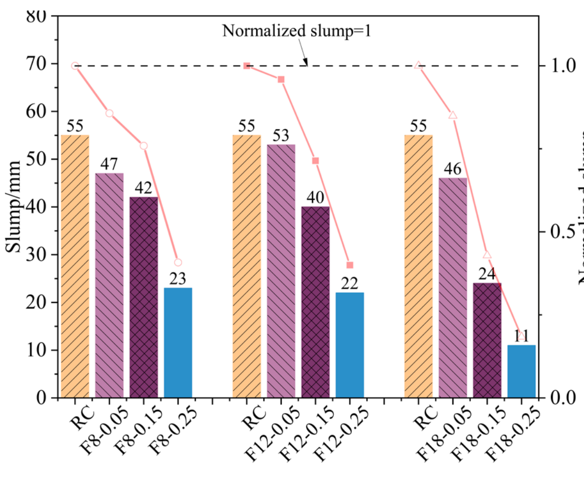

Figure 6. Comparative analysis of slump.

on the flexural characteristics of fiber-reinforced concrete. This phenomenon may be attributed to a balance between the diminished air entrainment caused by shorter fibers and their limited capacity to halt crack propagation (15).

To effectively analyze the impact of fiber parameters, length and dosage, on flexural strength (Fs), a multiple linear regression analysis (MLRA) was performed, and the findings are presented in Table 6. The significance of the analysis of variance (ANOVA) is less than 0.05, indicating that the model developed with independent variables and dependent variable is scientific. The significant coefficient (0.033) indicates that fiber length more significantly affects Fs than fiber dosage. However, at higher dosages, the positive impact of increased fiber length decreases. For example, Fs in F12-0.25 and F18-0.25 is 1.324 times greater than in normal concrete (NC), mainly due to fiber length enhancing microcrack suppression and distribution uniformity in the cement matrix. Longer fibers effectively prevent microcrack development, improving flexural strength. Yet, their tendency to cluster can reduce their effective length and create weak points in the concrete, potentially undermining the benefits of longer fibers (19). Moreover, the concrete's tensile stress is transferred to the fibers, resulting in an increase in the stress borne by the fibers and ultimately enhancing flexural performance (34). These phenomena can be also obtained from SEM analysis.

3.3. Cracking resistance

The cracking parameters (max width, max length, total area and index of anti-cracking) of all type mixtures are depicted in Figures 8 and 9. It is clear that PVA fiber significantly enhances cracking resistance compared to normal concrete (NC). As detailed in the partial enlarged view of Figure 8, the 12 mm fibers outperform both the 8 mm and 18 mm fibers in terms of crack parameters. Specifically, the maximum width, maximum length, and total area of cracks for the F12-0.25 series are reduced to 96.1%, 93.1%, and 92%, respectively, compared to NC. For the 8 mm series at a fiber volume fraction of 0.25%, the improvements are noted as 83.3%, 82.3%, and 86.4% in these parameters, respectively. Meanwhile, the 18 mm series shows increases of 92.3%, 91.9%, and 88.9% in these parameters under identical conditions. There is a positive correlation between the maximum width of a crack and the total area of cracking as depicted in Figures 8(a) and (c). Furthermore, Figure 9 shows that the crack resistance index varies with fiber length, with indices of 0.65, 0.99, and 0.95 for 8 mm, 12 mm, and 18 mm fibers at a 0.25% volume fraction, respectively.

Table 6. The key parameters of MLRA.

Model	Model adjusted r^2	Significance of ANOVA	Standardized coefficient		Significance of coefficient		VIF	
			PVA length	PVA dosage	PVA length	PVA dosage	PVA length	PVA dosage
1	0.871	0.000[c]	0.623	0.354	0.033	1.178	4.455	4.455

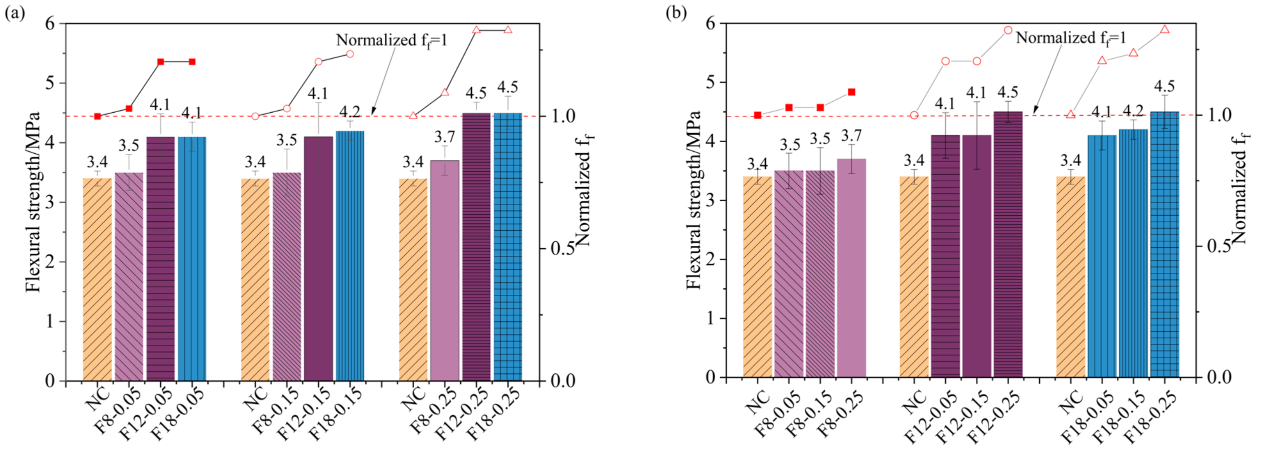

Figure 7. Fs of concrete: (a) the effect of PVA fiber lengths; (b) the effect of PVA fiber dosages.

The improvements in cracking resistance can be attributed to the interactions between PVA fibers and the cement matrix. When subjected to tensile stress from shrinkage, the fibers inhibit crack formation by providing shear resistance at the fiber-matrix interface (35). The length of the fibers plays a crucial role: shorter fibers might not bond effectively with the matrix, resulting in slippage and reduced crack resistance, whereas longer fibers enhance the contact area and strengthen the bond (36). Moreover, the high polarity of PVA fiber serves as nucleation sites for calcium ions, improving adhesion at the interface and consequently increasing crack resistance (37). This study finds that 12 mm PVA fiber is optimal, offering the best balance between adhesive forces and mechanical interlocking, essential for controlling crack propagation.

To evaluate the overall properties of fiber concrete, five dimensions were selected for evaluation: crack width, crack area, index of anti-cracking, flexural strength, and slump. It is evident from Figures 7 and 8 that Fs and anti-cracking are notably affected by the 0.25% fiber content. To further analyze performance variations with different fiber lengths, FX-0.25 was examined in Figure 10. It becomes apparent that concrete samples containing 12 mm and 18 mm PVA fibers demonstrate similar levels of performance in terms of flexural strength and index of anti-cracking. Specimens with 8 mm and 12 mm PVA fiber show comparable workability. By evaluating the graphical representations of these five dimensions, it is evident that the performance of the 12 mm specimen surpasses that of the 8 mm and 18 mm specimens.

3.4. Chloride penetration profiles

After the overall performance analysis, combining with the improved mechanical performance and resistance of cracking, only the performance of 12 mm series specimens was tested to characterize chloride penetration profiles.

3.4.1. Chloride penetration depth

The depth of chloride existence along with the varying time is depicted in Figure 11. It can be observed that the more time varies, the more deepened penetration it gains. The 0.25% volume fraction PVA fiber particularly alleviates the depth of chloride penetration after selected wetting-drying cycles. In particular, the depth is 1.9 mm, 2 mm, 4.4 mm and 4.8 mm corresponding to 28, 56, 84 and 112 days of drying-wetting cycle, respectively, which decreases 36.6%, 44.4%, 22.8% and 15.9% compared to the NC.

It is noteworthy that the change in chloride penetration depth for F12-0.25 after 28 and 56 days is minimal. This phenomenon is likely linked to the interaction between PVA fiber and hydration products,

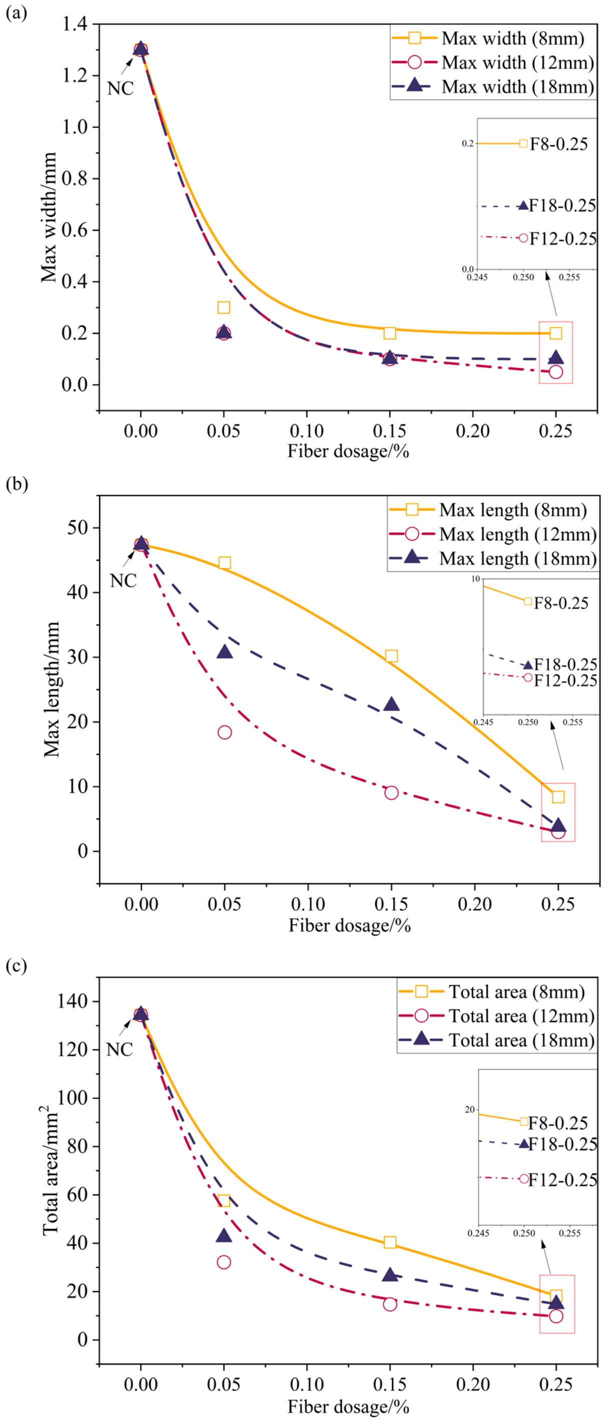

Figure 8. The parameters of cracking: (a) max width, (b) max length, (c) total area of cracking.

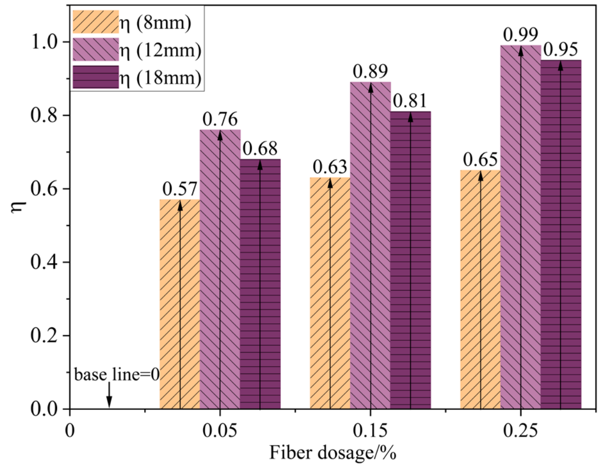

Figure 9. The index of anti-cracking.

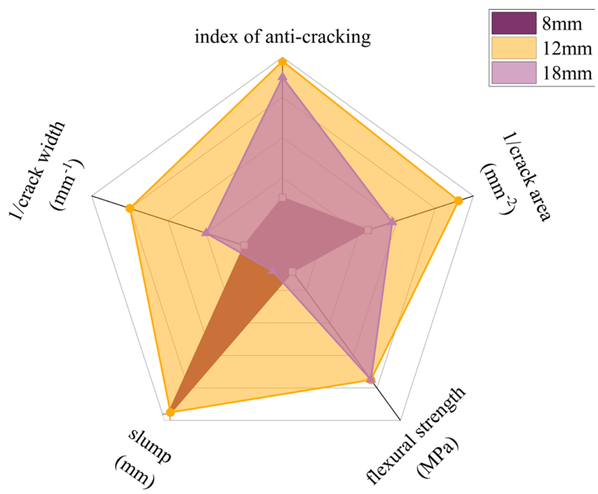

Figure 10. Five-dimensional representation of FX-0.25.

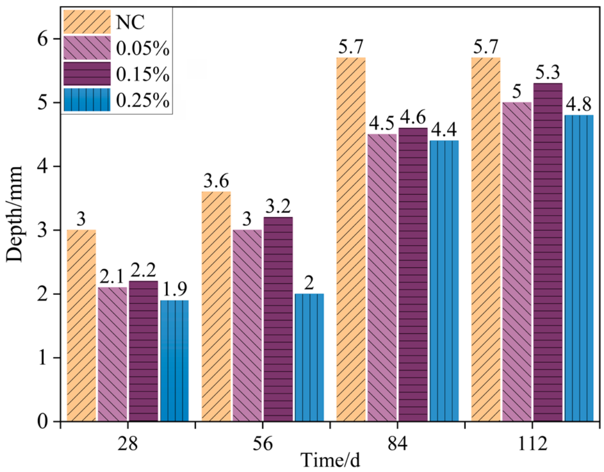

Figure 11. The depth of chloride penetration.

as well as the degree of hydration and erosion of the concrete. According to Coppola (38) and Wang (39), in the early stages of erosion, the depth of chloride penetration is associated with minor cracks formed between the PVA fiber structure and early hydration products. The minimal presence of microcracks resulting from specimen erosion leads to insignificant variations in chloride penetration for F12-0.25 after erosion periods of 28 and 56 days. Additionally, concerning the influence of time on chloride ion penetration, the depth of chloride penetration after an 84 days drying-wetting cycle is comparable to that after a 112-day cycle. This suggests that the temporal factor becomes less critical once the drying-wetting cycle exceeds a certain duration in this study.

3.4.2. Chloride penetration profiles

The chloride content distribution of PVA-FRC at three cyclic times in terms of 28, 56 and 112 days is depicted, as shown in Figure 12. The relationship between chloride content and depth, as shown in the as shown in figure 12(b) is non-linear, influenced by the concentration gradient and capillary action, as noted in references (40, 41). It is observed that the maximum chloride content does not coincide with the deepest point of chloride penetration. Instead, chloride content increases with penetration depth up to a peak point and then decreases beyond this point.

It is worth noting that after 112 days of cyclic service, the depth of the free chloride content is generally stabilized at 15 mm. At this depth, the free chloride ion concentrations in NC, F12-0.15, and F12-0.25 are 0.049%, 0.05%, and 0.041%, respectively. Notably, the highest concentration of free chloride ions is found at 3.5 mm after the 112-day period. The phenomenon that the maximum free chloride proportions appear at a certain depth in the specimen is called the wick effect (42). Clearly, the content of chloride ions and their penetration depth tend to decrease with increasing amounts of fiber in the concrete. The lowest peak chloride content is observed when the PVA fiber dosage is 0.25%, whereas the highest is at a dosage of 0.15% as shown in figure 12(a). This indicates that an optimal amount of fiber in the concrete can hinder chloride diffusion. Additionally, the different curves eventually align nearly parallel, suggesting that a higher fiber content does not alter the primary ion transport mechanism. This observation aligns with findings reported by Liu (43).

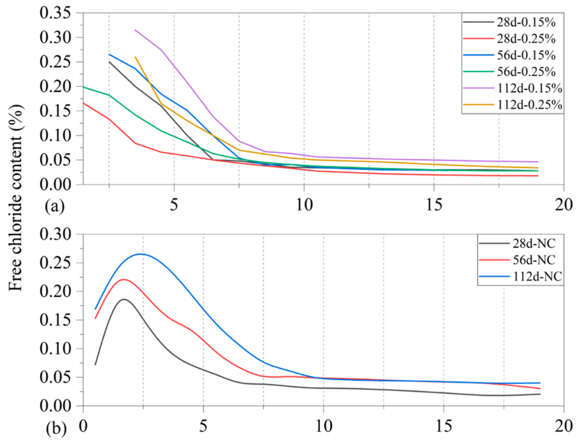

Figure 12. The chloride content distribution after cycles:

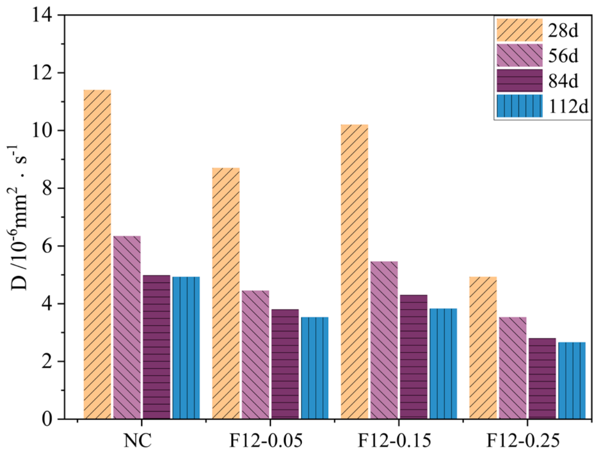

Figure 13. The coefficient of chloride diffusion in specimens.

3.4.3. Coefficient of chloride diffusion

According to the experimental results, the apparent chloride diffusion coefficients (D) of NC and 12 mm series specimen are calculated, which can be seen from Figure 13.

At the same erosion duration, the coefficient of chloride diffusion in NC is higher, compared to fiber concrete. The specimens with 0.25% fiber content show a diffusion coefficient that is 20.6-43.3% lower than those with 0.05% fiber content. F12-0.15 showed the highest chloride ion diffusion coefficient. This result is likely due to the highest air content and the largest pore structure at this fiber dosage. NMR analysis further confirms this finding. As shown in Figure 15(b), the total peak area is largest in the 0.15% series compared to other dosages, indicating increased porosity. F12-0.25 has the lowest value of the coefficient, which grabs the best chloride penetration resistance. It can be explained that D may depend on matrix cracking resistance as an utmost index of anti-cracking (η) elaborating in section Cracking resistance. In addition, this may be attributed to highly dense matrix with improved pore structure.

3.5. NMR

NMR techniques are sensitive enough to distinguish between different proton populations in concrete

(44). Free water in the inner concrete typically resides in air voids and cracks, while bound water is found in the capillary pores within the concrete. Consequently, NMR techniques can be employed to analyze the porosity of selected samples using T_2 spectrum curves.

The curves with various PVA fiber dosages and length are shown in Figure 14. For each PVA-FRC and NC, three signal peaks are basically displayed by T_2, except F18-0.05 with two peaks. The first signal peak occupies the mainly dominant position. Specifically, the first peak signal changes from 0.01 to 0.1, namely, two orders of magnitude of distribution. Particularly, at 0.25% dosage of PVA fiber, the emergence time of T_2 spectrum curve is earlier and the distributions of main signal peak are narrower with respect to the other group specimens. The above all indicates that the pores in the interior region of the concrete are mainly micro-pores (45), in this investigation.

The existence of porosity can be characterized by integrating the T_2 curve. To facilitate the comparation, the total area of peak of various specimens are normalized with the NC in Figure 15. Adding 0.05% and 0.15% to mixture, the content of small pores (i.e. the area of the main peak) is positively correlated with fiber dosage. Based on low dosage fiber, 18 mm PVA fiber plays a marginally negative role in the first signal peak area. The similar phenomenon also can be seen at specimens incorporating 12 mm PVA fiber. The negligible alteration in the peak area of F18-0.05 and F12-0.05 can also serve as an additional explanation for the absence of notable changes in 3.2. flexural strength. It is differential in relatively higher dosage groups. Adding 0.25% to mixture, the better performance of PVA-FRC is explained by T_2 spectrum in consideration of the total areas and signal peak ratio. The proportion of first signal peak and the total area of peak, regardless of PVA fiber length both undergo optimization. Compared to NC, F12-0.25 and F18-0.25 show improvements of 9.31% and 4.65%, as well as 54.61% and 35.25% in two parameters, respectively. This is a plausible explanation as to why the erosive properties of chlorine salts have increased with the addition of fibers. The refinement of the porosity, a declined total peak area and a ratio of first signal peak, can be observed.

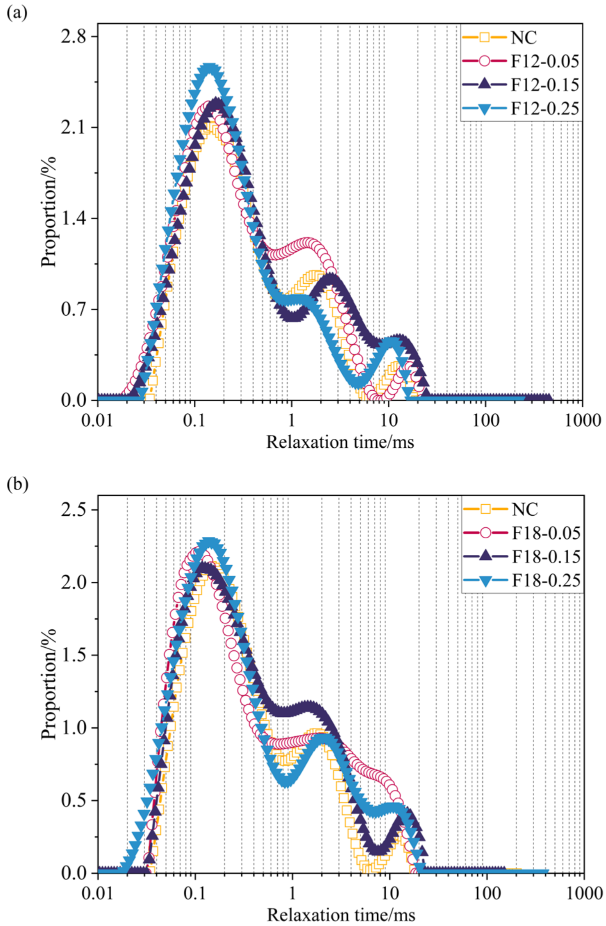

Figure 14. T2 spectrum curves of specimens: (a) 12 mm series (b) 18 mm series.

3.6. SEM

As the Figure 16 shown, PVA fiber tends to locally act as reinforcement through anchorage and confinement, and it possesses a rough surface. Moreover, the fiber plays a crucial role in the bridging mechanism, which helps impede the propagation of cracks. With a moderate dosage of PVA fiber, enhanced strength properties can be achieved due to the reduction in internal defects, as confirmed by the SEM image (Figure 16(b)). The process of fiber bridging and deflection contributes positively to improved mechanical properties and energy dissipation (46). Additionally, due to the hydroxyl group on the molecular chain, the PVA fiber acts as nucleus on which the hydrated production could grow (47). This interaction can be clearly seen in the way fibers are embedded within the matrix, enhancing the bonding between the surrounding mortar and the fibers, as visualized in (48). These characteristics yield significant effect to present better mechanical properties and durability performances.

4. CONCLUSIONS

The study conducted investigated the mechanical characteristics, cracking resistance, and chloride diffusion performance of PVA-FRC, taking into account variations in PVA fiber dosage and length. The conclusions are summarized as follows:

1. Incorporation of PVA fiber reduces workability of the concrete, significantly decreasing the slump

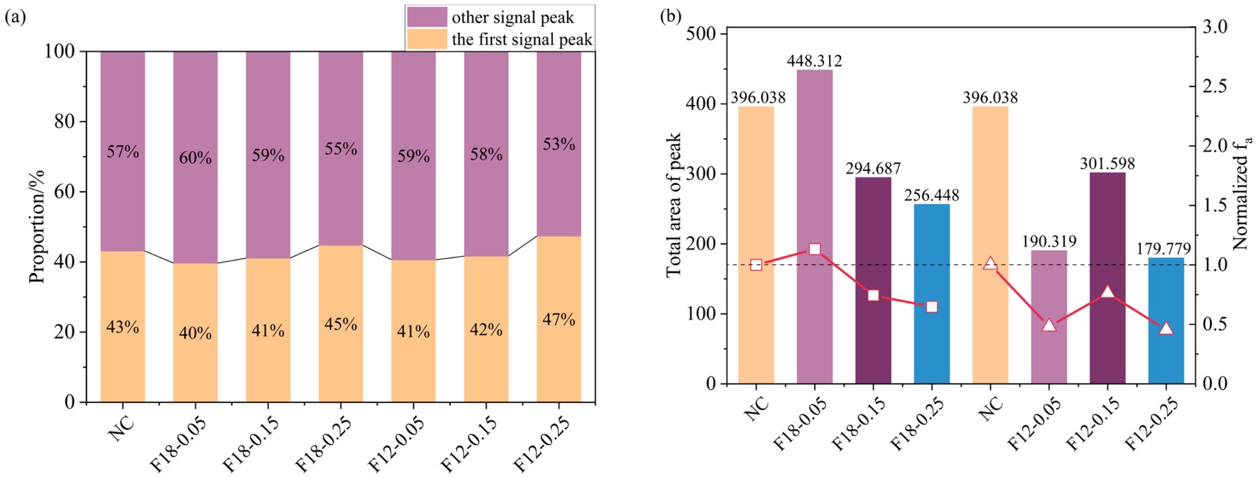

Figure 15. The area distribution of T_2 spectrum curves: (a) proportion of the first signal peak; (b) total area of peak.

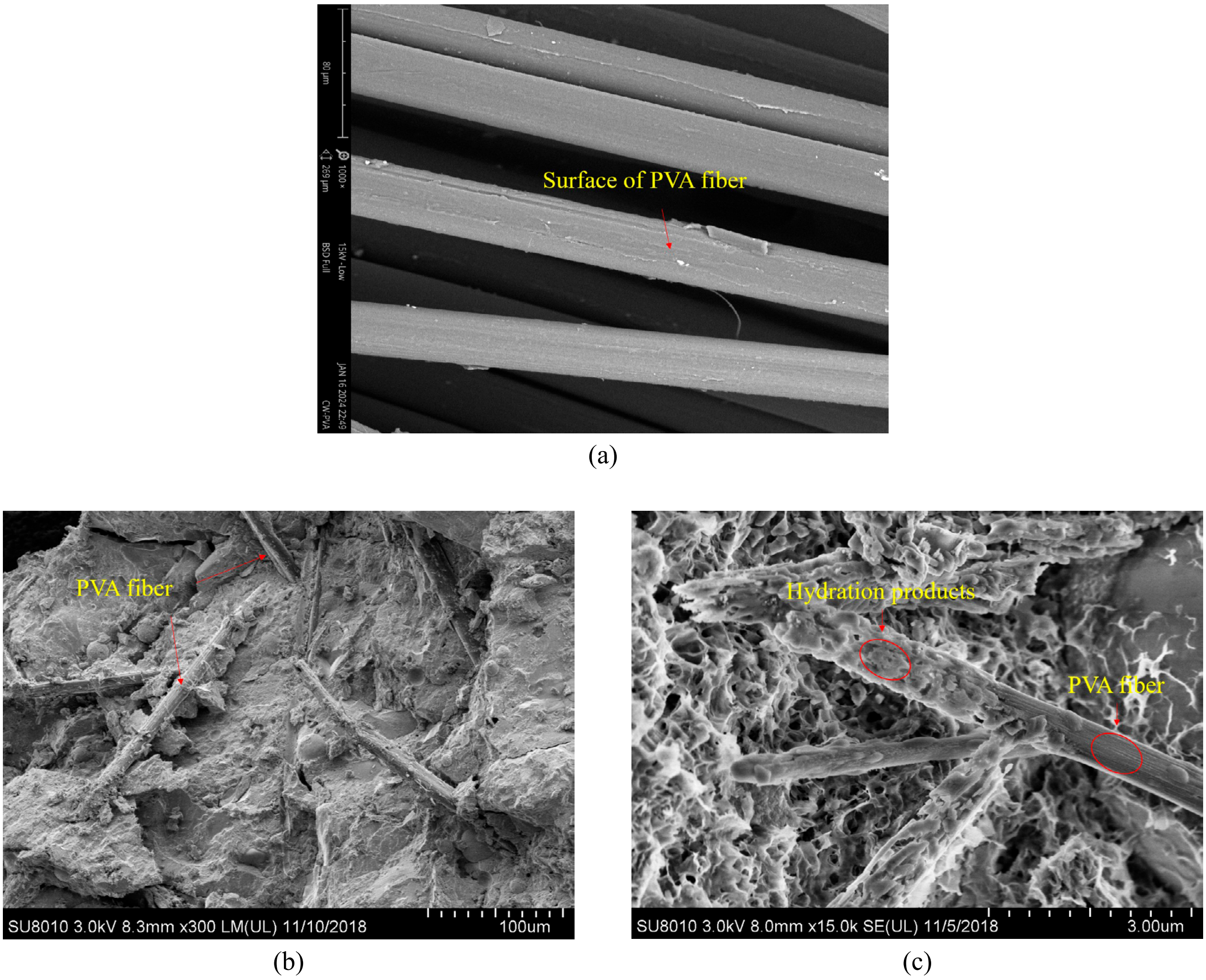

Figure 16. (a) The rough surface of fiber, (b) fiber bridging performance and random distribution of fiber in concrete, (c) bonding between fiber and hydration products.

value compared to normal concrete. Longer fibers at a volume fraction of 0.25% exacerbate this reduction in workability.

2. PVA fiber significantly enhances the flexural strength of concrete. The optimal flexural performance is achieved with fibers measuring 18 mm in length at a 0.25% volume fraction, where strength is 1.324 times that of normal concrete (NC). Fiber length influences flexural strength more markedly than fiber dosage.
3. PVA fiber with a length of 12 mm demonstrates superior performance in reducing crack dimensions, such as maximum width and length, and total crack area, compared to fibers of 8 mm and 18 mm lengths. Relative to NC, the maximum improvements in crack resistance parameters with 12 mm fibers are 96.1%, 93.1%, and 92%, respectively.
4. PVA fiber contributes to enhancing concrete's resistance against chloride ion penetration. The depth of chloride penetration stabilizes after a duration of 112 days, showing consistent results at earlier time points (28 and 56 days).
5. Increasing the dosage of fibers optimizes the proportion of the first signal peak and the total peak area in measured results, regardless of the fiber length. Notably, with dosages of 0.25%, fibers of 12 mm and 18 mm lengths show improvements of 9.31% and 4.65% in the first peak, and 54.61% and 35.25% in the total peak area, respectively.
6. After a comprehensive evaluation of durability and mechanical properties, the study recommends a PVA-FRC mixture with 0.25% fiber dosage and 12 mm fiber length. This formulation is suggested for further applications due to its optimized performance characteristics.

Acknowledgments

The authors are grateful for the contribution of the Hohai university and Inner Mongolia University of Science & Technology.

Authorship contribution statement

Wei Chen: Data Curation, Formal analysis, Investigation, Methodology, Resources, Software, Validation, Visualization, Writing-original draft, Writing-review & editing.

Yang Wen: Conceptualization, Funding acquisition, Methodology, Project administration, Resources, Supervision, Validation.

Declaration of competing interest

The authors of this article declare that they have no financial, professional or personal conflicts of interest that could have inappropriately influenced this work.

REFERENCES

1. Afroughsabet V, Ozbakkaloglu T. 2015. Mechanical and durability properties of high-strength concrete containing steel and polypropylene fibers. Constr. Build. Mater. 94:73-82. https://doi.org/10.1016/j.conbuildmat.2015.06.051
2. Kizilkanat AB, Kabay N, Akyüncü V, Chowdhury S, Akça AH. 2015. Mechanical properties and fracture behavior of basalt and glass fiber reinforced concrete: An experimental study. Constr. Build. Mater. 100:218-224. https://doi.org/10.1016/j.conbuildmat.2015.10.006
3. Zhang J, Gong C, Guo Z, Zhang M. 2009. Engineered cementitious composite with characteristic of low drying shrinkage. Cem. Concr. Res. 39(4):303-312. https://doi.org/10.1016/j.cemconres.2008.11.012
4. Uygunoğlu T. 2008. Investigation of microstructure and flexural behavior of steel-fiber reinforced concrete. Mater. Struct. 41(8):1441-1449. https://doi.org/10.1617/s11527-007-9341-y
5. Wang Y, Liu Z, Wang Y, Wang D, Yuan C, Liu R. 2022. Effect of recycled aggregate and supplementary cementitious material on the chloride threshold for steel bar corrosion in concrete. Constr. Build. Mater. 346:128418. https://doi.org/10.1016/j.conbuildmat.2022.128418
6. Daneshfar M, Hassani A, Aliha M, Berto F. 2017. Evaluating mechanical properties of macro-synthetic fiber-reinforced concrete with various types and contents. Strength Mater. 49:618-626. https://doi.org/10.1007/s11223-017-9907-z
7. Noushini A, Samali B, Vessalas K. 2013. Effect of polyvinyl alcohol (PVA) fibre on dynamic and material properties of fibre reinforced concrete. Constr. Build. Mater. 49:374-383. https://doi.org/10.1016/j.conbuildmat.2013.08.035
8. Kale V, Shelar A, Javanjal V, Gadhave S, Munde K, Sharma A. 2023. Experimental study on fiber reinforced concrete using PVA fiber and glass powder. Mater. Today Proc. https://doi.org/10.1016/j.matpr.2023.10.155
9. Li VC, Wang S, Wu C. 2001. Tensile strain-hardening behavior of polyvinyl alcohol engineered cementitious composite (PVA-ECC). Mater. J. 98(6):483-492. https://doi.org/10.14359/10851
10. Xu B, Toutanji H A, Gilbert J. 2010. Impact resistance of poly (vinyl alcohol) fiber reinforced high-performance organic aggregate cementitious material. Cem. Concr. Res. 40(2):347-351. https://doi.org/10.1016/j.cemconres.2009.09.006
11. Toutanji H, Xu B, Gilbert J, Lavin T. 2010. Properties of poly (vinyl alcohol) fiber reinforced high-performance organic aggregate cementitious material: Converting brittle to plastic. Constr. Build. Mater. 24(1):1-10. https://doi.org/10.1016/j.conbuildmat.2009.08.023
12. Cao M, Si W, Xie C. 2020. Relationship of rheology, fiber dispersion, and strengths of polyvinyl alcohol fiber-reinforced cementitious composites. ACI Mater. J. 117(3):191-204. https://doi.org/10.14359/51724598
13. Hu W, Yang X, Zhou J, Xing H, Xiang J. 2013. Experimental research on the mechanical properties of PVA fiber reinforced concrete. Res. J. Appl. Sci. Eng. Technol. 5(18):4563-4567. https://doi.org/10.19026/rjaset.5.4375
14. Jang JG, Kim H, Kim T, Min B, Lee H. 2014. Improved flexural fatigue resistance of PVA fiber-reinforced concrete subjected to freezing and thawing cycles. Constr. Build. Mater. 59:129-135. https://doi.org/10.1016/j.conbuildmat.2014.02.040

15. Wang L, Zhou S, Shi Y, Tang S, Chen E. 2017. Effect of silica fume and PVA fiber on the abrasion resistance and volume stability of concrete. Compos. B. Eng. 130:28-37. https://doi.org/10.1016/j.compositesb.2017.07.058

16. Wu Y, Song W, Zhao W, Tan X. 2018. An experimental study on dynamic mechanical properties of fiber-reinforced concrete under different strain rates. Appl. Sci. 8(10):1904. https://doi.org/10.3390/app8101904

17. Lin H. 2006. Research on the performance of mechanics and deformation of concrete with PVA fiber. Master thesis. Nanjing University of Aeronautics and Astronautics.

18. Zhang Z, Feng J, Li J, Zhu Z, Pan Y, Zhao Q. 2024. Damage prediction for tunnel lining considering mechanical behaviour of fibre reinforced concrete with action of train loading. Eur. J. Environ. Civ. Eng. 1-41. https://doi.org/10.1080/19648189.2024.2318420

19. Pujadas P, Blanco A, Cavalaro S, Aguado A. 2014. Plastic fibres as the only reinforcement for flat suspended slabs: Experimental investigation and numerical simulation. Constr. Build. Mater. 57:92-104. https://doi.org/10.1016/j.conbuildmat.2014.01.082

20. CECS 38-2004 2004. Technical specification for fiber reinforced concrete structures. China Stand.

21. GB/T 50080-2016. 2016. Standard for test method of performance on ordinary fresh concrete. China Stand.

22. Li M, Li V C. 2013. Rheology, fiber dispersion, and robust properties of engineered cementitious composites. Mater. Struct. 46:405-420. https://doi.org/10.1617/s11527-012-9909-z

23. Yang Y. 2002. Methods study on dispersion of fibers in CFRC. Cem. Concr. Res. 32(5):747-750. https://doi.org/10.1016/s0008-8846(01)00759-1

24. CECS 13-2009. 2009. Standard test methods for fiber reinforced concrete. China Stand

25. Castellote M, Andrade C, Alonso C. 1999. Chloride-binding isotherms in concrete submitted to non-steady-state migration experiments. Cem. Concr. Res. 29(11):1799-1806. https://doi.org/10.1016/s0008-8846(99)00173-8

26. JTS/T 236-2019. 2019. Technical specification for concrete testing of port and waterway engineering. China Stand.

27. Valori A, McDonald PJ, Scrivener KL. 2013. The morphology of C-S-H: Lessons from 1H nuclear magnetic resonance relaxometry. Cem. Concr. Res. 49:65-81. https://doi.org/10.1016/j.cemconres.2013.03.011

28. Freedman R. 2006. Advances in NMR logging. J. Pet. Technol. 58(01):60-66. https://doi.org/10.2118/89177-ms

29. Zhang P, Zheng Y, Wang K, Zhang K. 2020. Combined influence of nano-$CaCO_3$ and polyvinyl alcohol fibers on fresh and mechanical performance of concrete incorporating fly ash. Struct. Concr. 21(2):724-734. https://doi.org/10.1002/suco.201900134

30. Noushini A, Vessalas K, Samali B. 2014. Static mechanical properties of polyvinyl alcohol fibre reinforced concrete (PVA-FRC). Mag. Concr. Res. 66(9):465-483. https://doi.org/10.1680/macr.13.00320

31. Yew MK, Bin Mahmud H, Ang BC, Yew MC. 2015. Effects of low volume fraction of polyvinyl alcohol fibers on the mechanical properties of oil palm shell lightweight concrete. Adv. Mater. Sci. Eng. 2015(1):425236. https://doi.org/10.1155/2015/425236

32. Zhang Y, Sun W, Li Z. 2008. Effect of PVA short fiber and fly ash on rheological and flexural behaviors of geopolymer composites. Acta Materiae Compositae Sinica. 25(6):166-174. https://doi.org/10.13801/j.cnki.fhclxb.2008.06.025

33. Si W, Cao M, Li L. 2020. Establishment of fiber factor for rheological and mechanical performance of polyvinyl alcohol (PVA) fiber reinforced mortar. Constr. Build. Mater. 265:120347. https://doi.org/10.1016/j.conbuildmat.2020.120347

34. Xu H, Shao Z, Wang Z, Cai L, Li Z, Jin H, Chen T. 2020. Experimental study on mechanical properties of fiber reinforced concrete: Effect of cellulose fiber, polyvinyl alcohol fiber and polyolefin fiber. Constr. Build. Mater. 261:120610. https://doi.org/10.1016/j.conbuildmat.2020.120610

35. Zhang P, Li Q-f. 2013. Effect of polypropylene fiber on durability of concrete composite containing fly ash and silica fume. Compos. B. Eng. 45(1):1587-1594. https://doi.org/10.1016/j.compositesb.2012.10.006

36. Festugato L, Menger E, Benezra F, Kipper EA, Consoli NC. 2017. Fibre-reinforced cemented soils compressive and tensile strength assessment as a function of filament length. Geotext. Geomembr. 45(1):77-82. https://doi.org/10.1016/j.geotexmem.2016.09.001

37. Shoji D, He Z, Zhang D, Li VC. 2022. The greening of engineered cementitious composites (ECC): A review. Constr. Build. Mater. 327:126701. https://doi.org/10.1016/j.conbuildmat.2022.126701

38. Coppola L, Coffetti D, Crotti E. 2018. Plain and ultrafine fly ashes mortars for environmentally friendly construction materials. Sustain. 10(3):874. https://doi.org/10.3390/su10030874

39. Wang J, Dong H. 2023. PVA fiber-reinforced ultrafine fly ash concrete: Engineering properties, resistance to chloride ion penetration, and microstructure. J. Build. Eng. 66:105858. https://doi.org/10.1016/j.jobe.2023.105858

40. Chen C, Wang L, Liu R, Zhu P, Liu H, Wang X, Yu J, Chen Y. 2023. Chloride penetration of concrete exposed to dry-wet cycle with various dry-wet ratios and temperature. Constr. Build. Mater. 400:132883. https://doi.org/10.1016/j.conbuildmat.2023.132883

41. Cao J, Jin Z, Ding Q, Xiong C, Zhang G. 2022. Influence of the dry/wet ratio on the chloride convection zone of concrete in a marine environment. Constr. Build. Mater. 316:125794. https://doi.org/10.1016/j.conbuildmat.2021.125794

42. Andrade C, Climent M, De Vera G. 2015. Procedure for calculating the chloride diffusion coefficient and surface concentration from a profile having a maximum beyond the concrete surface. Mater. Struct. 48(4):863-869. https://doi.org/10.1617/s11527-015-0543-4

43. Liu F, Ding W, Qiao Y. 2019. An experimental investigation on the integral waterproofing capacity of polypropylene fiber concrete with fly ash and slag powder. Constr. Build. Mater. 212:675-686. https://doi.org/10.1016/j.conbuildmat.2019.04.027

44. Xu F, Wang S, Li T, Liu B, Li B, Zhou Y. 2021. Mechanical properties and pore structure of recycled aggregate concrete made with iron ore tailings and polypropylene fibers. J. Build. Eng. 33:101572. https://doi.org/10.1016/j.jobe.2020.101572

45. Liu L, He Z, Cai X, Fu S. 2021. Application of low-field NMR to the pore structure of concrete. Appl. Magn. Reson. 52(1):15-31. https://doi.org/10.1007/s00723-020-01229-7

46. Arain MF, Wang M, Chen J, Zhang H. 2019. Experimental and numerical study on tensile behavior of surface modified PVA fiber reinforced strain-hardening cementitious composites (PVA-SHCC). Constr. Build. Mater. 217:403-415. https://doi.org/10.1016/j.conbuildmat.2019.05.083

47. Su Y, Qian C, Rui Y, Feng J. 2021. Exploring the coupled mechanism of fibers and bacteria on self-healing concrete from bacterial extracellular polymeric substances (EPS). Cem. Concr. Compos. 116:103896. https://doi.org/10.1016/j.cemconcomp.2020.103896

48. Khan M, Cao M, Ali M. 2020. Cracking behaviour and constitutive modelling of hybrid fibre reinforced concrete. J. Build. Eng. 30:101272. https://doi.org/10.1016/j.jobe.2020.101272